

We are IntechOpen, the world's leading publisher of Open Access books Built by scientists, for scientists

5,300

Open access books available

130,000

International authors and editors

155M

Downloads

Our authors are among the

154

Countries delivered to

TOP 1%

most cited scientists

12.2%

Contributors from top 500 universities



WEB OF SCIENCE™

Selection of our books indexed in the Book Citation Index
in Web of Science™ Core Collection (BKCI)

Interested in publishing with us?
Contact book.department@intechopen.com

Numbers displayed above are based on latest data collected.
For more information visit www.intechopen.com



Chapter

Osmium Containing Double Perovskite Ba_2XOsO_6 ($\text{X} = \text{Mg}, \text{Zn}, \text{Cd}$): Important Candidates for Half-Metallic Ferromagnetic and Spintronic Applications

Sajad Ahmad Dar

Abstract

In this chapter, Osmium-based double perovskites Ba_2XOsO_6 ($\text{X} = \text{Mg}, \text{Zn}, \text{Cd}$) have been investigated for their magnetic structure, electronic, elastic, mechanical and thermodynamic belongings. These materials have been recently reported experimentally for their magnetic structure. Here, we report the first successful ab initio calculations on the physical properties of these materials. The structural optimization for these Ba_2XOsO_6 ($\text{X} = \text{Mg}, \text{Zn}, \text{Cd}$) double perovskite compounds has been finalized within density functional theory via full potential linearized augmented plane wave (FP-LAPW) method. The structural investigation exposes the ferromagnetic phase stability of these compounds. The spin-polarized electronic and magnetic properties were calculated within generalized gradient approximation (GGA), Hubbard approximation (GGA+U) and modified Becke-Johnson approximation (mBJ). The electronic profile establishes the half-metallic nature for all the three compounds. The total spin magnetic moment was found to be an integer value of $2 \mu_B$. The elastic constants have been calculated and used to predict mechanical stuffs like Shear modulus (G), Poisson ratio (ν) and anisotropic factor. The calculated B/G and Cauchy pressure ($C_{12}-C_{44}$) both characterize these materials as brittle. The thermodynamic parameters like heat capacity and Debye temperature have been predicted in the temperature range of 0–1000 K.

Keywords: Ba_2XOsO_6 ($\text{X} = \text{Mg}, \text{Zn}, \text{Cd}$), spintronics, ferromagnetic, elastic, mechanical behavior, thermodynamics

1. Introduction

The need of advanced materials with novel properties for industrial and technological use has strained the material community to have a deep and appropriate understanding of the periodic table elements, along with their combinations. Therefore, materials community consequently observes the vital changes in innovative designing of novel materials. A tremendous increase in simulation power, along with algorithmic improvements in quantum theory allows one to have

well-organized and exact quantum mechanical calculations. This has hence stretched the computing power to such extent that those properties of materials which were once observed extremely difficult are now easily being calculated with a great precision [1, 2]. From last few years work on perovskites especially double perovskites has geared up due to their vast technological applications and displaying multifunctional properties. The general formula of perovskites is looked as ABO_3 , where “A” and “B” are cations and “O” is oxygen anion. The charge of “A” and “B” cations can vary in the original Perovskite. Double perovskites are potential members of this diverse perovskite family having different structures, composition and properties. The double perovskite compounds having a general formula $A_2BB'O_6$ have benefited the material community because of great technological applications including spintronic materials, multi-ferroic materials, half-metallic materials, ferromagnetic materials, magneto-dielectric materials, magneto-optic materials, insulating ferrimagnetism [3–8]. The double perovskite family exhibits a wide range of magnetic behaviors, like actually simple antiferromagnets presented by (Ba_2LiOsO_6) , ferromagnets $(Ba_2MgReO_6$ and $Ba_2NaOsO_6)$, spin singlet ground states for (Ba_2YMoO_6) , and spin glasses (Sr_2CaReO_6) [9–13]. Osmium based double perovskites especially Sr_2FeOsO_6 , $SrFeCaOsO_6$, Ca_2FeOsO_6 have been extensively investigated for puzzling magnetic behavior [14–19]. Perovskites with ABO_3 structure like $BaPuO_3$, $SrPuO_3$, $BaAmO_3$, $SrAmO_3$, $EuGaO_3$, $EuInO_3$ etc. have been reported for spintronic applications [20–24]. Further materials like $BaMoO_3$, $SrMoO_3$, $XReO_3$ ($X = Rb, Cs, Tl$), $SnTaO_3$, $PbMoO_3$ [25–28] have been recently reported for fuel cell applications. Numerous investigations have also been reported on halide perovskites for solar cell applications like $MAPbBr_3$ and $MAPbI_3$ [29–36].

Ba_2XOsO_6 ($X = Mg, Zn, Cd$) cubic double perovskites have been recently reported in space group $Fm-3m$ (225). The complete details of the respective experimental lattice parameters are given in **Table 1**. The Ba atoms are located at $8c$ ($1/4, 1/4, 1/4$) of the unit cell, X atoms are at position $4b$ ($0.5, 0.5, 0.5$), Os atoms are positioned at $41a$ ($0, 0, 0$) and O atoms at $24e$ ($X, 0, 0$) ($X = 0.233, 0.238, 0.234$)

Parameter	Present	Other	Present	Other	Present	Other
	Ba_2MgOsO_6		Ba_2ZnOsO_6		Ba_2CdOsO_6	
Lattice Constant	8.1548	8.07 [37] 8.08 [61] 8.06 [61]	8.19	8.09 [37] 8.09 [61] 8.06 [61]	8.388	8.31 [37] 8.325 [61]
Volume	914.90		929.62		995.96	
B	150.93		144.23		140.14	
B'	4.44		4.13		4.7	
Bond length						
Os-O	1.95		1.95		2.00	
Mg, Zn, Cd-O	2.11		2.15		2.18	
Ba-Ba	4.07		4.10		4.19	
Ba, Mg, Zn, Cd	3.53		3.55		3.62	
Os-Mg, Zn, Cd	4.07		4.10		4.19	
E_0	-68425.9		-71617.3		-79217.0	

Table 1. Optimized ground states parameters for all the three osmium double perovskites.

respectively for Mg, Zn, Cd [37]. Further double perovskites of the variant A₂BB'O₆ like Ba₂MgReO₆, Sr₂MnTaO₆, Ba₂InTaO₆ and many more have also been reported for electronic, magnetic, mechanical, optical, thermoelectric and thermodynamic investigations [38–47]. As far Ba₂XOsO₆ (X = Mg, Zn, Cd) compounds are concerned which belongs to the same variant not much attention has been paid towards these perovskites so far, regarding the above mentioned characteristic properties. Hence, in the present work an attempt to predict the properties for these double perovskite has been made and to check out their potential applications. The most successful density functional theory (DFT) has been employed for the investigation of magnetic, electronic, elastic, mechanical and thermo-physical behavior. For the investigation of thermo-physical behavior quasi harmonic Debye model [48, 49] has been used for the prediction of important parameters like specific heat, thermal expansion, Debye temperature, Grüneisen parameter etc.

2. Computational details

The computational technique used during the calculations process is based on full-potential linearized augmented plane wave (FP-LAPW) [50] method based upon density functional theory (DFT) [51] as employed in WIEN2K. For structural optimization generalized gradient approximation (GGA) scheme of Perdew, Burke and Ernzerhof (PBE) [52] has been used. For electronic and magnetic calculations in addition to (GGA), Hubbard approximation (GGA + U) [45] and modified Becke-Johnson (mBJ) [53] has been used. For GGA + U approach the incorporation U- term can be done by various methods [54, 55]. In the present work we have used self-interaction correction method (SIC) [56] as implemented in WIEN2K. The value of U_{eff} was varied from 1 to 5 eV and J was set to 0, so as to properly adjust the Os-d in density of states. The final U value used throughout the calculations was set to 2.00 eV [57]. For precise energy convergence the value of R_{MT}K_{max} was taken 7, where R_{MT} is the small atomic radius in unit cell and K_{max} denotes the size of the largest **k** vector in the plane wave expansion. The value of L_{max} was taken as 10, and G_{max} = 12 (a.u.)⁻¹. The energy and charge convergence criterion is considered when the total energy is stable within 0.001 Ry and the charge difference is less than 0.001e/a.u.³ per unit cell. A mesh of 1000 K points is considered for Brillouin zone integration via tetrahedral method [58]. The elastic constants were calculated using the scheme developed by Charpin [59] as integrated in WIEN2K package. The thermodynamic parameters have been calculated using quasi-harmonic Debye model [48, 49] for the pressure and temperature dependency of some essential thermodynamic parameters. In this model the Gibbs function takes the form;

$$G^*(V, P, T) = E(V) + P(V) + F_{vib}(\theta(V); T) \quad (1)$$

where E(V), P(V), $\theta(V)$ are the total energy per unit cell, the constant hydrostatic pressure and Debye temperature respectively and F_{vib} is the vibration term written as;

$$F_{vib}[\theta(V); T] = N K_B T \left[\frac{9\theta}{8T} + 3 \ln \left(1 - e^{-\frac{\theta}{T}} \right) - D\left(\frac{\theta}{T}\right) \right] \quad (2)$$

$D\left(\frac{\theta}{T}\right)$ in equation represents the Debye integral, N is the number of atoms per formula unit, K_B the Boltzmann's constant. The Debye temperature θ_D is expressed as;

$$\theta_D = \frac{h}{K_B} \left(6\pi^2 V^{1/2} N \right)^{1/3} f(v) \sqrt{\frac{B_s}{M}} \quad (3)$$

In the above equation B_s represents the adiabatic bulk modulus, M is the molecular mass per unit cell, the bulk modulus is expressed by

$$B_s = V \left(\frac{d^2 E(V)}{dV^2} \right) \quad (4)$$

The non-equilibrium Gibbs function $G^*(V, P, T)$ can be minimized with respect to volume V ;

$$\left[\frac{dG^*(V; P, T)}{dV} \right]_{P, T} \quad (5)$$

Solution of Eq. (5) gives a detailed information about the thermodynamic quantities like thermal expansion α , heat capacity at constant volume C_V , heat capacity at constant pressure C_P , given respectively by;

$$\alpha = \frac{\gamma C_V}{B_T V} \quad (6)$$

$$C_V = 3nk \left[4D \left(\frac{\theta_D}{T} \right) - \frac{3\theta_D/T}{e^{\theta_D/T} - 1} \right] \quad (7)$$

$$C_P = C_V (1 + \gamma \alpha T) \quad (8)$$

In Eq. (8) γ represents the Grüneisen parameter, which is approximated as

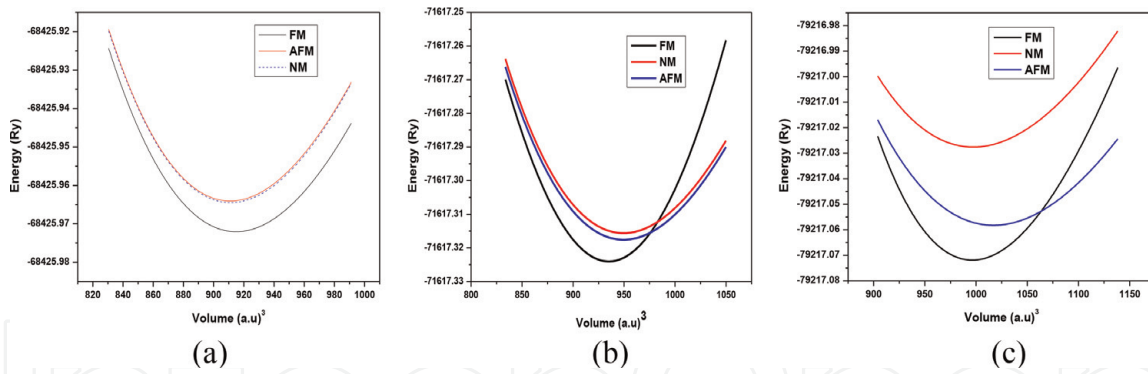
$$\gamma = - \frac{d \ln \theta_D(V)}{d \ln V} \quad (9)$$

3. Results and discussion

3.1 Structural properties

The optimized volume for all the three compounds has been made by fitting the total energy as a function of its cell volume using Birch–Murnaghan’s equation of state [60]. Marjerrison et al. [37] have recently reported all the three compounds in cubic B1-phase space group Fm-3 m (225). The Ba atoms are located at position 8c (0.25, 0.25, 0.25), Mg, Zn, Cd at 4b (0.5, 0.5, 0.5), Os at 4a (0, 0, 0) and O atoms are sited at 24e (X, 0, 0) (X = 0.233, 0.238, 0.234) respectively for Mg, Zn, Cd. The geometry and structural optimization has been carried in Non-magnetic (NM), ferromagnetic (FM), and anti-ferromagnetic (AFM) phases. The ground state energy was found lowest for all the three compounds in the ferromagnetic phase as presented in **Figure 1(a–c)**, and thus a stable configuration.

The optimized ground state lattice constants are close to available experimental and theoretical results. The ground state parameters like bulk modulus (B_0), lattice constant (a_0) pressure derivatives of bulks modulus and energy are grouped in **Table 1**.

**Figure 1.**

Energy versus volume for ferromagnetic (FM), non-magnetic (NM) and anti-ferromagnetic (AFM) cases (a) Ba_2MgOsO_6 (b) Ba_2ZnOsO_6 (c) Ba_2CdOsO_6 .

3.2 Elastic and mechanical properties

In the present work the Charpin method has been employed for the calculation of elastic constants C_{ij} (C_{11} , C_{12} , C_{44}) values as implemented in WIEN2K. The values of elastic constants were obtained by calculating the total energy as a function of volume-conserving strains. The value of the elastic constants and mechanical properties are summed up in **Table 2**. The calculated values of elastic constants properly satisfy the criteria for cubic elastic constants and ensures the stability $C_{11}-C_{12} > 0$, $C_{11} > 0$, $C_{44} > 0$, $(C_{11} + 2C_{12}) > 0$, $C_{12} < B < C_{11}$ [47]. The Poisson's ratio (ν), Young's modulus (E), and Shear modulus (G) are calculated by using [62–64] and presented in **Table 2**. According to Hill [65] average shear modulus, G is defined as arithmetic mean of Voigt, G_V and Reuss, G_R values. Young's modulus (E) deals with the stiffness of the material. The obtained value of (E) was found to be 215.75, 190.82, 169.83 GPa respectively for Ba_2XOsO_6 ($X = Mg, Zn, Cd$). Thus large value of (E) provides a clear indication that these compounds will behave as tough materials. Ba_2MgOsO_6 has the largest value of (E) as compared to other

GGA	$BaMgOsO_6$	$BaZnOsO_6$	Ba_2CdOsO_6
C_{11}	262.60	240.70	232.07
C_{12}	86.90	98.85	84.32
C_{44}	84.10	76.91	61.66
B	150	145.59	132.95
G_V	85.61	74.51	66.54
G_R	85.57	74.39	66.02
G	85.50	74.45	66.28
E	215.75	190.82	169.83
ν	0.2617	0.2815	0.2871
B/G	1.7652	1.95	2.00
$C_{12}-C_{44}$	2.8	21.94	22.66
A	0.957	1.08	0.8346
T_m	2105 ± 300	2100 ± 300	1925 ± 300

Table 2.

Calculated elastic constants C_{11} , C_{12} , C_{44} in (GPa), bulk modulus B (GPa), shear modulus G (GPa), Young's modulus E (GPa), Poisson's ratio ν , Zener anisotropy factor a, B/G ratio, Cauchy pressure $C_{12}-C_{44}$ and melting temperature T_m (K) for Ba_2XOsO_6 ($X = Mg, Zn, Cd$).

perovskites under consideration in this study. The reason for the decreasing value of (E) is the Bulk modulus which has also a decreasing trend as one goes with X position from Mg to Cd via Zn. The B/G ratio is the measure of ductility and brittleness of a material. According to Pugh [66], a material is brittle if the ratio $B/G < 1.75$ and is ductile if $B/G > 1.75$. The B/G ratio for Ba_2XOsO_6 (X = Mg, Zn, Cd), was calculated to be 1.765, 1.95, 2.00 respectively, which is higher than the limit value for all the three compounds, thus all the three compounds will show ductile nature. Cauchy pressure ($C_{12}-C_{44}$) also helps to estimate the ductility and brittleness of a material. The positive value of ($C_{12}-C_{44}$) portrays a material as ductile and negative value as brittle. The calculated value was also found to be positive for all the three compounds. Hence both B/G value and Cauchy pressure verifies the ductile nature for all the three perovskites Ba_2XOsO_6 (X = Mg, Zn, Cd).

Zener anisotropy factor 'A' is the property of a material to show altered characteristic in various direction of its structure. As per this a material is isotropic if and only if 'A' factor has unit value or otherwise anisotropic. The calculated value of 'A' for the compound was found to 0.975, 1.08, 0.83 which is less than unity for Ba_2MgOsO_6 and Ba_2CdOsO_6 and greater than unity for Ba_2ZnOsO_6 , hence in all the three cases deviating from unity, thus the materials will present anisotropic nature. Poisson's ratio (ν) describes the nature of bonding forces. The upper and lower limits of Poisson's ratio are 0.25 and 0.50 [20–24]. The (ν) value varies from material to material. For covalent materials, (ν) has a typical value of 0.1, for ionic materials (ν) = 0.25 and for metallic materials the value (ν) = 0.33. The value of Poisson's ratio for Ba_2XOsO_6 (X = Mg, Zn, Cd) was calculated to be 0.261, 0.281 and 0.287 respectively, which lies close to 0.25 and hence suggest a higher ionic behavior as inter-atomic bonding for these compounds. The obtained values of elastic constants have also been used to predict, one important thermodynamic parameter known as melting temperature [26–28]. The calculated value of melting temperature was found 2100 ± 300 , 2105 ± 300 , 1925 ± 300 K respectively for Ba_2XOsO_6 (X = Mg, Zn, Cd). The calculated values of elastic constants, mechanical properties including melting temperature are grouped in **Table 2**.

3.3 Electronic and magnetic properties

For electronic structure calculations spin resolved band structure and density of states have been plotted using different correlation potentials. GGA calculated lattice parameter has been used to plot band structure and density of states within GGA, GGA + U and mBJ. These band structures and density plots usually deliver a decent understanding of the electronic contour of a material. The combination of different methods for band structure and density of state plots has been done as to understand the variation of results within different correlations. **Figures 2(a–c)**, **3(a–c)** and **4(a–c)** represent the spin included band structures within GGA, GGA + U and mBJ respectively for Ba_2XOsO_6 (X = Mg, Zn, Cd).

It is clear from these figures that the band profile for all the three compounds at the Fermi level is almost similar for all the approximation, presenting 100% of spin polarization. The Fermi level is set at 0 eV, separating the valance band maximum (VBM) from the conduction band minimum (CBM) in all figures. For spin up states the Fermi level remains fully occupied presenting metallic nature for all the three compounds and for spin down states the Fermi level remains completely vacant falling in a gap and thus generating a gap between (VBM) and (CBM), presenting the semi-conducting nature for the compounds. In case of Ba_2MgOsO_6 within GGA, GGA + U and mBJ respectively, the (VBM) lies on symmetry points ' Γ ' at -1.30 eV, -1.1 eV and -1.3 eV, and CBM lies on symmetry point ' X ' at 0.001, 0.7 and 1.2 eV respectively within GGA, GGA + U and mBJ. Hence in all the three cases the (VBM)

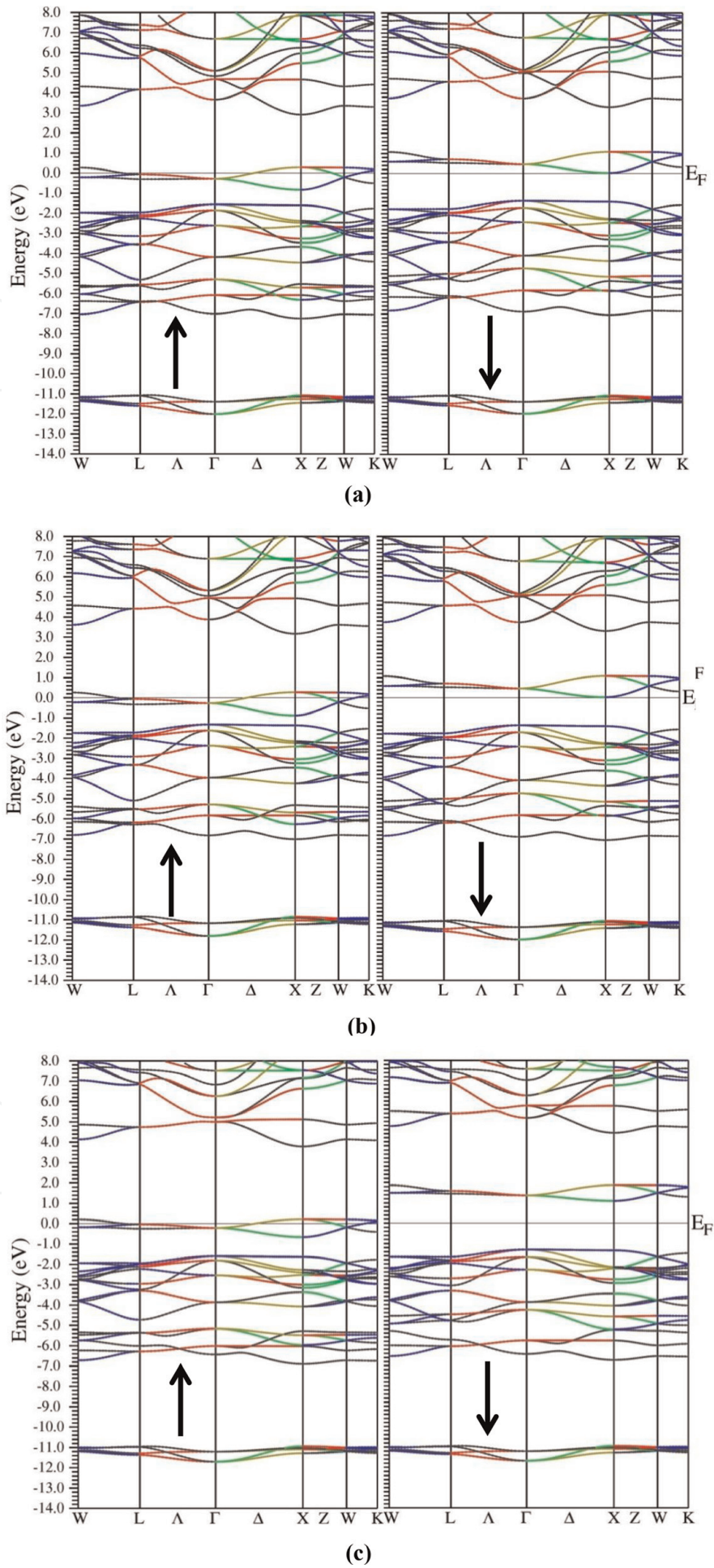


Figure 2.
Band structure left spin up and right spin down states within (a) GGA (b) GGA + U (c) mBJ for Ba_2MgOsO_6 .

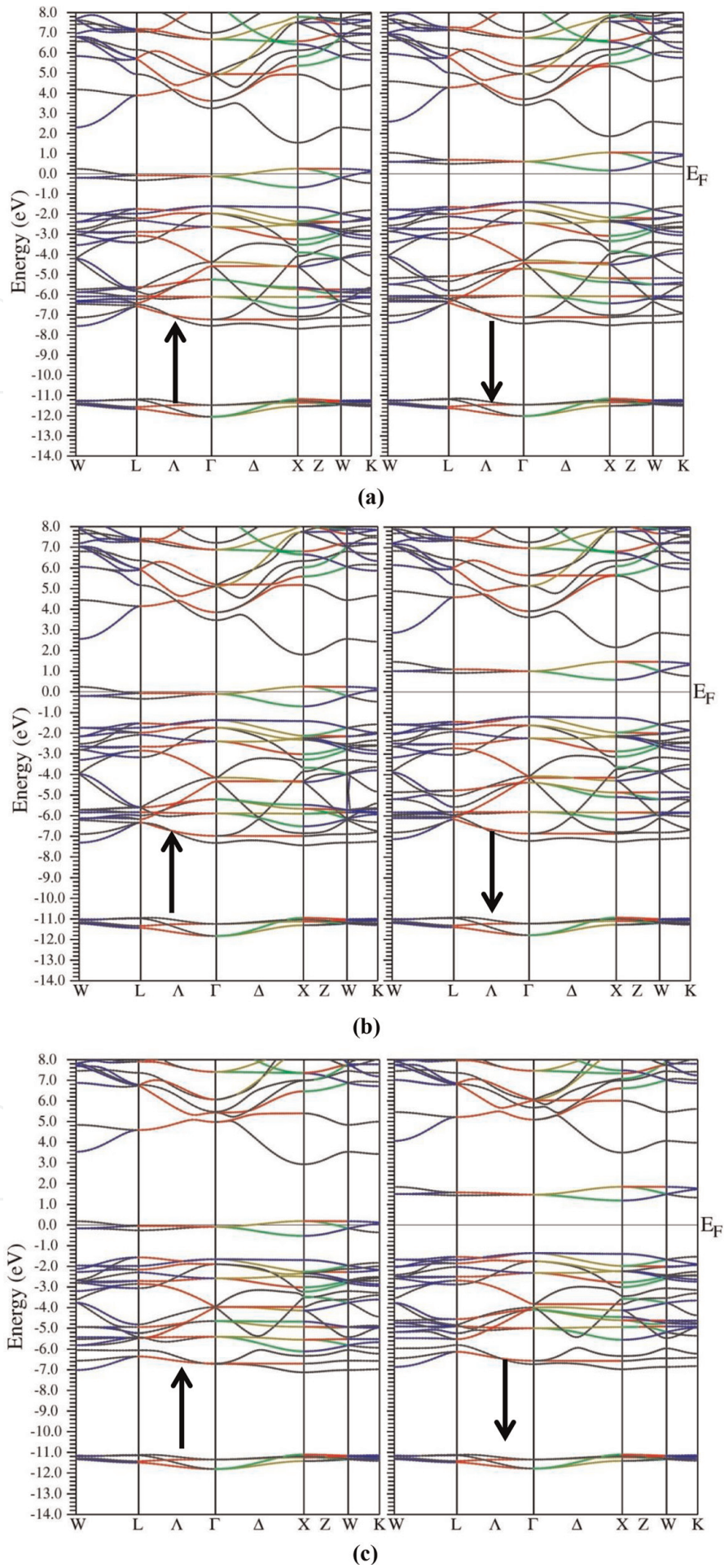


Figure 3. Band structure left spin up and right spin down states within (a) GGA (b) GGA + U (c) mBJ for Ba_2ZnOsO_6 .

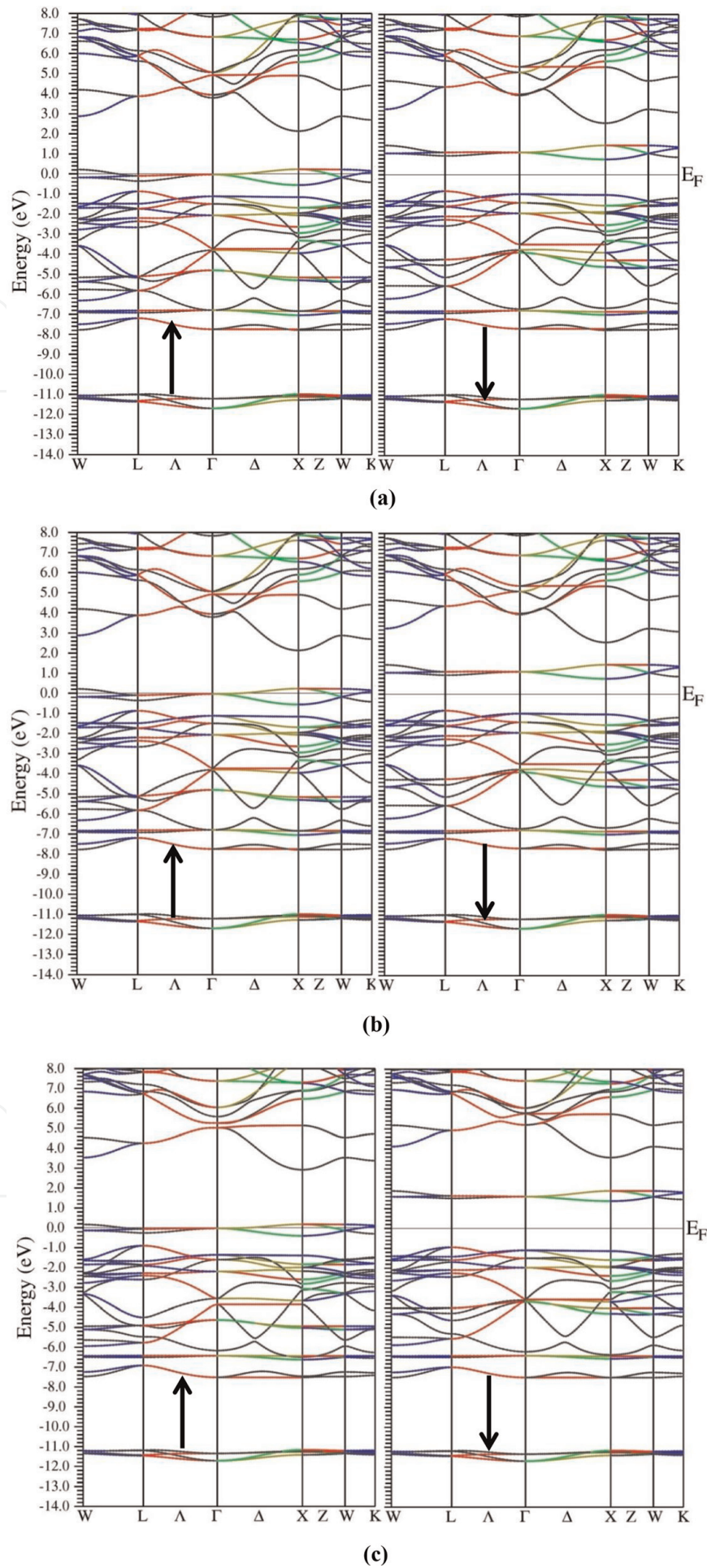


Figure 4.
Band structure of left spin up and right spin down (a) GGA (b) GGA + U (c) mBJ for Ba_2CdOsO_6 .

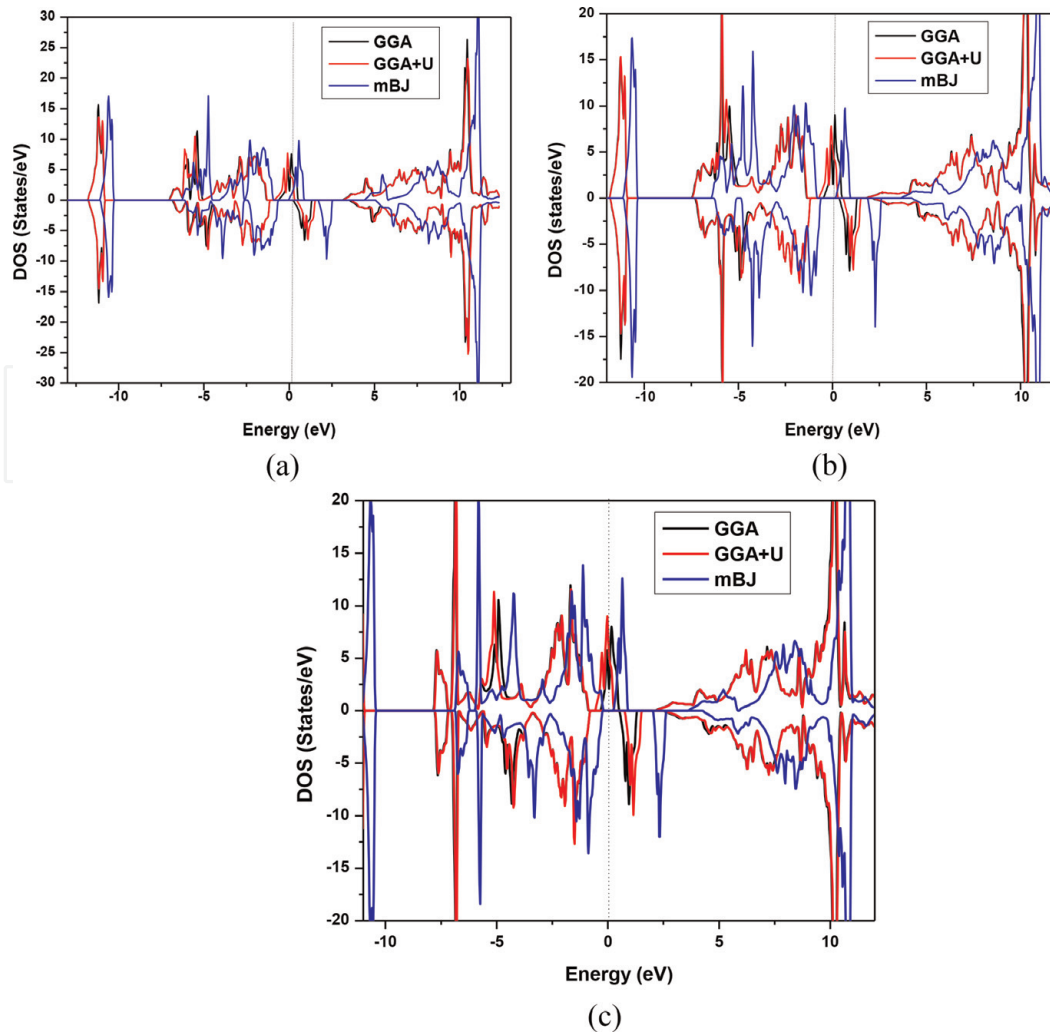


Figure 5. Combined DOS diagram for spin up and down states within GGA, GGA + U and mBJ (a) Ba_2MgOsO_6 (b) Ba_2ZnOsO_6 (c) Ba_2CdOsO_6 .

and (CBM) lie on ‘ Γ ’ and X point making the compound indirect band gap semiconductor in spin down states. The band gap value changes as we apply U and mBJ, the value of band gap found in GGA, GGA + U and mBJ are 1.3, 1.8 and 2.5 eV respectively for Ba_2MgOsO_6 . For Ba_2ZnOsO_6 the valance band maxima (VBM) lie on symmetry points ‘ Γ ’ at -1.40 , -1.2 , -1.4 eV respectively in GGA, GGA + U and mBJ, and the conduction band minimum (CBM) lies on symmetry point ‘X’ at 0.2 , 0.7 , and 1.0 eV respectively in GGA, GGA + U and mBJ, thus generating an indirect band gap of 1.6 , 1.9 and 2.4 eV respectively for GGA, GGA + U and mBJ. Similarly for Ba_2CdOsO_6 the valance band maxima (VBM) lie on symmetry points ‘L’ at -1.00 , -0.8 , -0.9 eV respectively in GGA, GGA + U and mBJ, the conduction band minimum (CBM) lies on symmetry point ‘X’ at 0.5 , 0.8 , and 1.4 eV respectively in GGA, GGA + U and mBJ, thus generating an indirect band gap of 1.5 , 1.6 and 2.3 eV respectively for GGA, GGA + U and mBJ. Thus from the band structure calculations 100% of spin polarization at Fermi level is observed. The compounds behave as metallic for spin up states and semi-conducting for spin down states. The overall band picture presents half-metallic nature for all the three compounds.

For the further explanation of the band picture, total density of states (TDOS) and partial density of states (PDOS) have been plotted. The spin included combined TDOS shown in **Figure 5(a-c)** disclose the same results as presented by band structure plots presenting metallic nature for spin up states and semi-conducting for spin down states for all the three approximations and hence overall half-metallic nature. The DOS peaks are found to increase in case of GGA + U and mBJ.

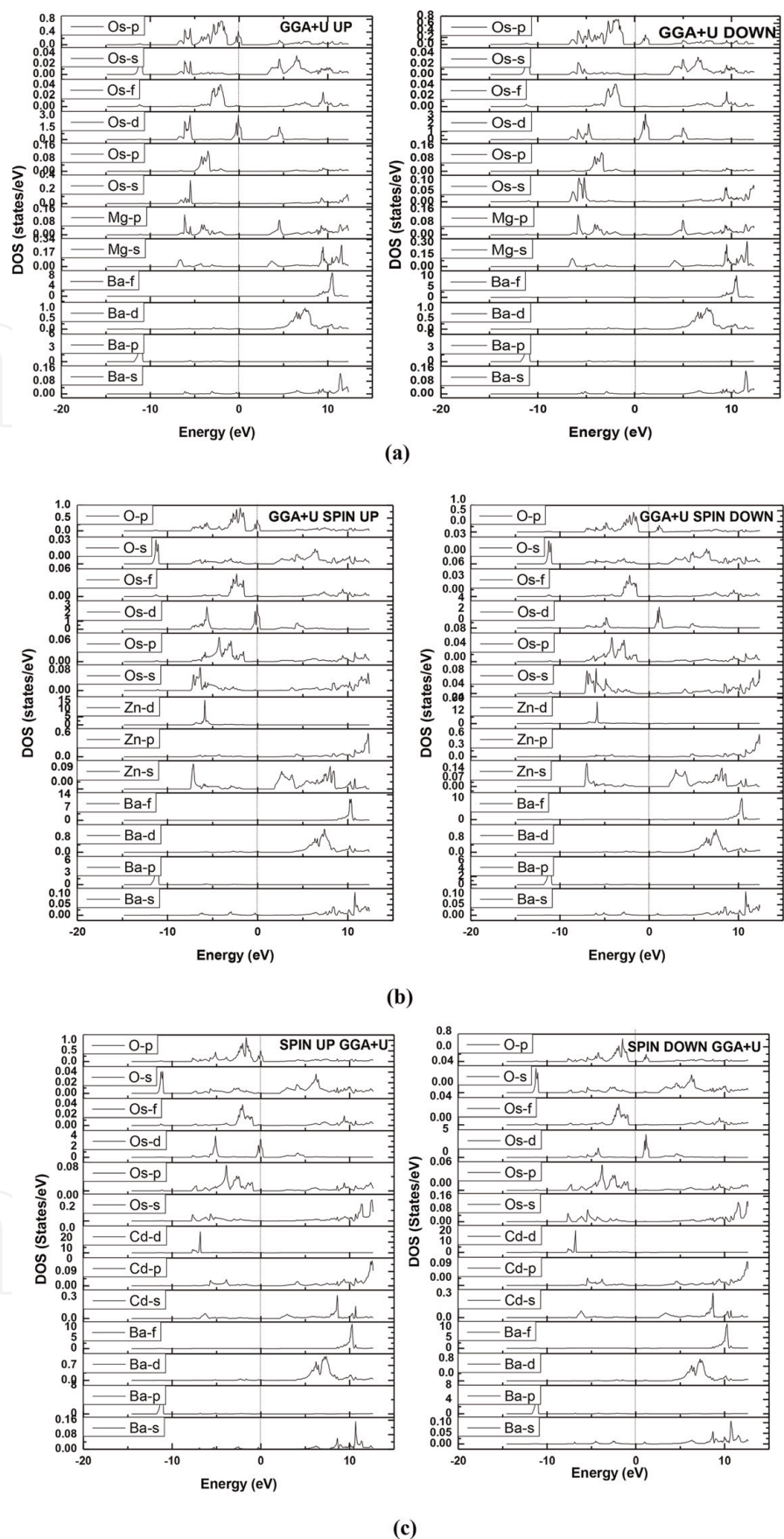


Figure 6. Partial density of states contribution in spin up and down states within GGA + U (a) Ba_2MgOsO_6 (b) Ba_2ZnOsO_6 (c) Ba_2CdOsO_6 .

The contribution to the TDOS picture has been represented by the partial contribution to the DOS diagram as depicted in **Figure 6(a–c)** for both spin up and down states within GGA + U. The (PDOS) has been plotted for (Ba-‘s’, ‘p’, ‘d’, ‘f’),

(Mg- 's', 'p', Zn-'s', 'p', 'd'), (Cd-'s', 'p', 'd'), (Os- 's', 'p', 'd', 'f') and O-'s', 'p' states. From these figures, it is clear that the metallic nature in spin up states for the compound in all the approximations is due to the Os-'d' states which are present at Fermi level with a small contribution of O-'p' states hybridized with one another and in case of spin down these 'd'- states of Os and 'p'-states of O are pulled inside the conduction band, thereby generating a gap in spin down states. Thus the spin included band profile, TDOS and PDOS results display that Ba_2XOsO_6 ($X = Mg, Zn, Cd$) all present half-metallic nature.

In order to check the magnetic nature of the compounds the total and partial magnetic moments have been calculated with GGA, GGA + U and mBJ. The total magnetic contribution is obtained as the summation of the partial moments of individual elements and the interstitial moments. The total magnetic moment obtained in all approximations is nearly same for all the compounds Ba_2XOsO_6 ($X = Mg, Zn, Cd$) equal to an integer value $2 \mu_B$ shown in **Table 3**. The main contribution to the total magnetic moment is mostly found from Osmium atoms. The partial moment of Os element shows a great variation on the application of Hubbard U and mBJ potentials. Hence it is clear that the ferromagnetic nature and large value of total magnetic moment for Ba_2XOsO_6 ($X = Mg, Zn, Cd$) is mainly due to Os atoms. The values of interstitial, partial and total magnetic moments are present in **Table 3**. Thus the large and integer value of magnetic moment of $2 \mu_B$ further verifies the half-metallic and ferromagnetic nature for Ba_2MgOsO_6 . The integer value of magnetic moment is one of the criteria for the half-metallic nature of a compound [22, 23].

3.4 Thermodynamic properties

In order to check the thermodynamic behavior quasi-harmonic Debye approximation [26–28] has been employed to check the temperature and pressure variation of some noteworthy thermodynamic quantities like heat at constant volume (C_V), thermal expansion (α), Grüneisen parameter (γ), Debye temperature (θ_D) and also the bulk modulus variation for these double perovskites. The variation of these parameters has been investigated under pressure and temperature. The temperature has been varied from 0 to 1000 K and pressure ranges from 0 to 15 GPa, with the step size of 5 GPa pressure. In this range of temperature quasi harmonic Debye model remains unconditionally valid.

Figure 7(a–c) presents the variation of bulk modulus (B) with temperature at different pressure points respectively at 0, 5, 10, and 15 GPa. Our results present a clear decrease in bulk modulus with temperature and an increase is observed with

Compound	Method	M_{int}	M_{Ba}	$M_{Mg,Zn,Cd}$	M_{Os}	M_O	M_{Tot}
Ba_2MgOsO_6	GGA	0.38	0.01	0.00	1.14	0.07	2.0
	GGA + U	0.35	0.01	0.00	1.25	0.06	2.0
	mBJ	0.22	0.00	0.00	1.41	0.05	2.0
Ba_2ZnOsO_6	GGA	0.37	0.01	0.00	1.15	0.07	2.0
	GGA + U	0.34	0.01	0.00	1.26	0.06	2.0
	mBJ	0.21	0.00	0.00	1.42	0.05	2.0
Ba_2CdOsO_6	GGA	0.37	0.01	0.00	1.18	0.06	2.0
	GGA + U	0.33	0.00	0.00	1.31	0.05	2.0
	mBJ	0.20	0.00	0.00	1.49	0.04	2.0

Table 3.

Calculated magnetic moment for Ferro-magnetic Ba_2XOsO_6 ($X = Mg, Zn, Cd$). Within GGA, GGA + U and mBJ (in Bohr magneton μ_B).

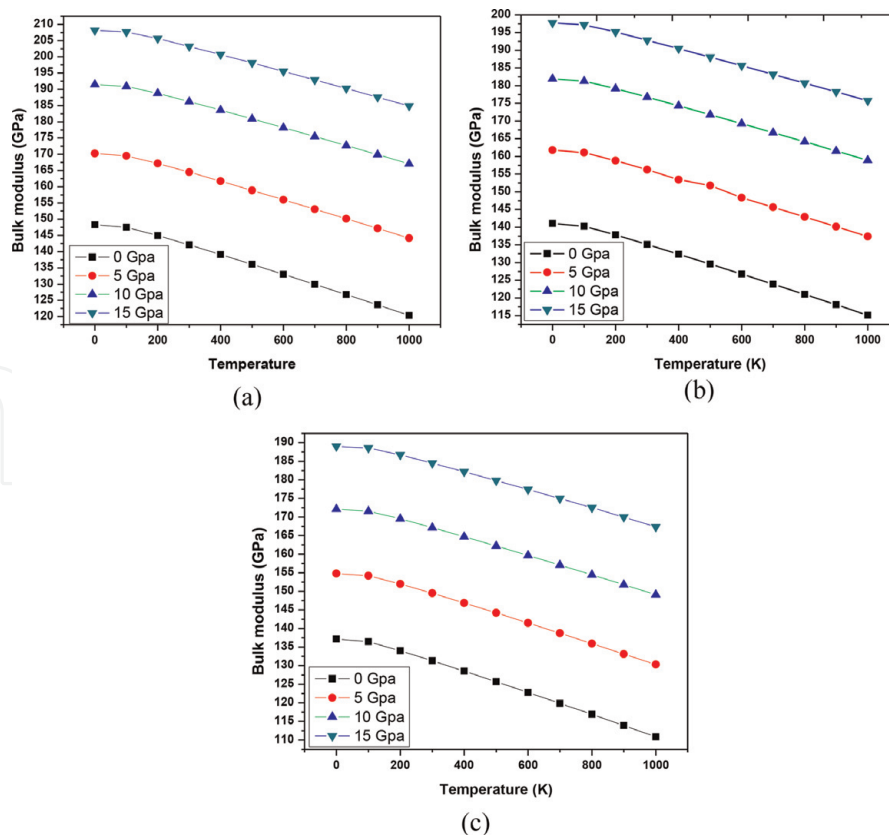


Figure 7.
 Dependence of bulk modulus on temperature and pressures for (a) Ba_2MgOsO_6 (b) Ba_2ZnOsO_6
 (c) Ba_2CdOsO_6 .

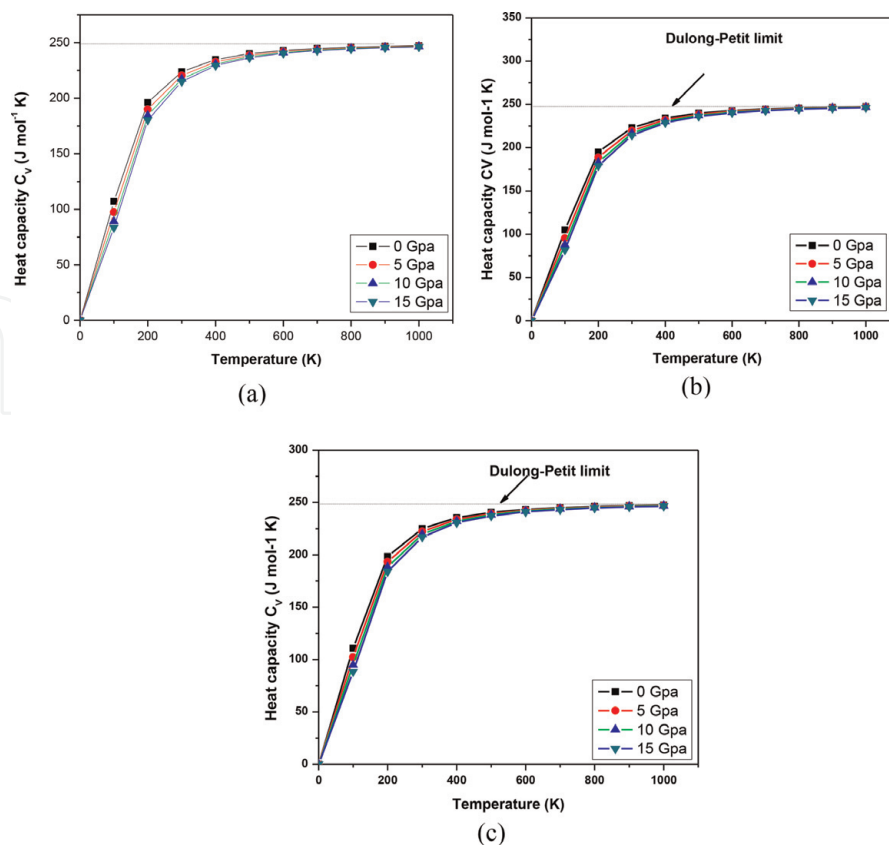


Figure 8.
 Dependence of specific heat (C_V) on temperature and pressures for (a) Ba_2MgOsO_6 (b) Ba_2ZnOsO_6
 (c) Ba_2CdOsO_6 .

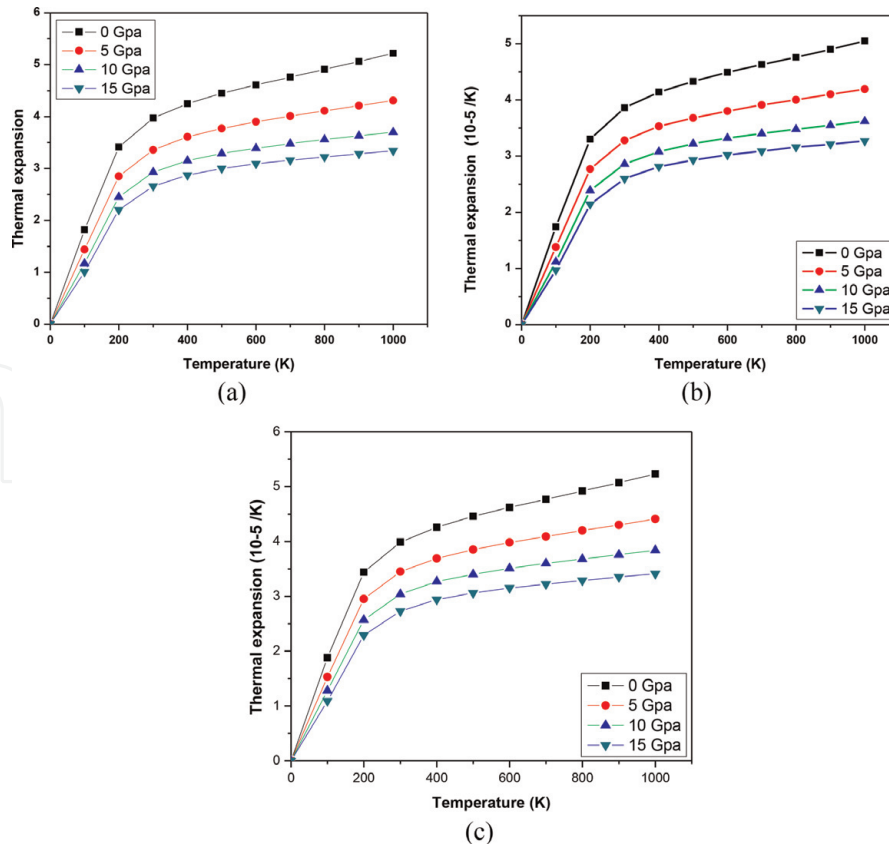


Figure 9.

Dependence of thermal expansion (α) on temperature and pressures for (a) Ba_2MgOsO_6 (b) Ba_2ZnOsO_6 (c) Ba_2CdOsO_6 .

pressure at different temperature values. The reason for this decrease of bulk modulus with temperature is that temperature reduces the hardness of a material, while pressure tends to increase the same.

Figure 8(a–c) depicts the variation of specific heat at constant volume (C_V) with temperature and pressure. One can have a clear understanding from the **Figure 8(a–c)** that the escalation of C_V is rapid under the lower temperature values of 0–300 K, but above 300 K a lethargic increase in C_V can be seen, which further becomes constant at high temperature at about 800 K beyond which, it follows the famous Dulong-Petit limit [67]. This variation of C_V for solids is a common observation. The calculated value of C_V at 300 K and 0 GPa of pressure for Ba_2XOsO_6 ($X = Mg, Zn, Cd$) was found to be 223.89, 223.16, 225.04 J mol⁻¹ K respectively.

Figure 9(a–c) shows the pressure and temperature dependence of thermal expansion coefficient, ' α ' respectively for Ba_2XOsO_6 ($X = Mg, Zn, Cd$). It is clear from the figure that the value of ' α ' increase with increasing temperature, the increase in ' α ' is found to be rapid under low temperatures values and under higher temperatures values a sluggish increase in ' α ' is observed. The main reason for the sluggish increase of ' α ' under high temperature values may be the saturation of ' α ' beyond 300 K. Pressure has a reverse effect on ' α ', increasing pressure decreases the ' α '. Under high pressure values ' α ' falls rapidly, same as the increase is observed under low temperatures.

Grüneisen parameter (γ) describes the variation in vibrational frequency of a lattice under the influence of temperature and pressure [68]. Pressure and temperature variation of (γ) for Ba_2XOsO_6 ($X = Mg, Zn, Cd$) is plotted in **Figure 10(a–c)**. The value of (γ) increases with increasing temperature and under pressure a reverse is observed, pressure decreases the value of (γ) and has a lowest value at 15 GPa of

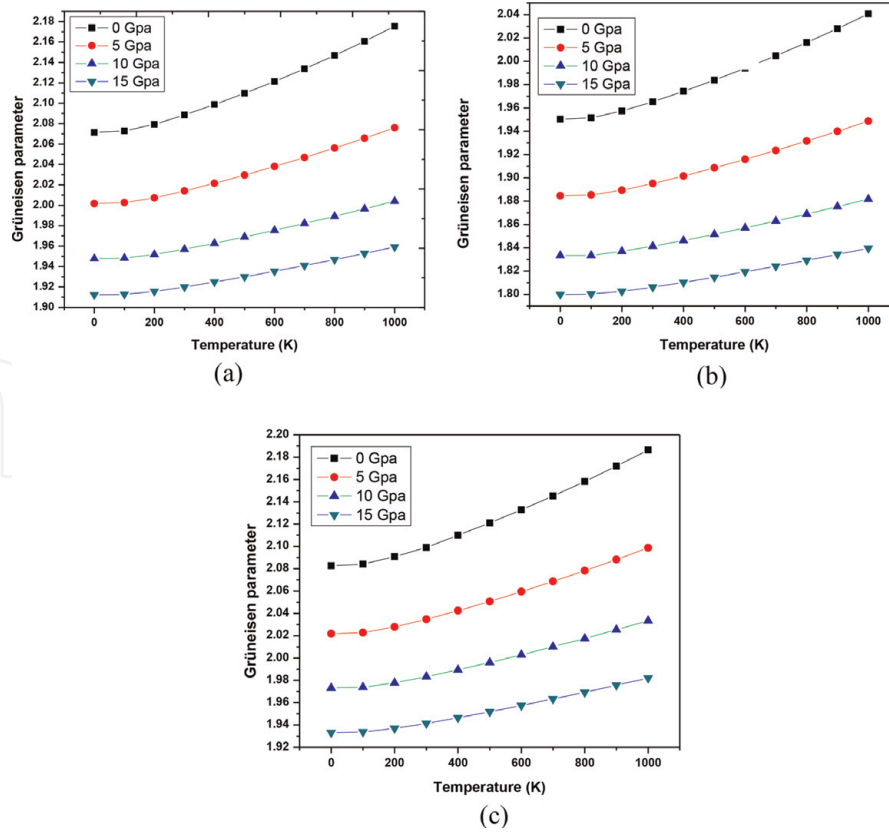


Figure 10.
 Dependence of Grüneisen parameter (γ) on temperature and pressures for (a) Ba_2MgOsO_6 (b) Ba_2ZnOsO_6 (c) Ba_2CdOsO_6 .

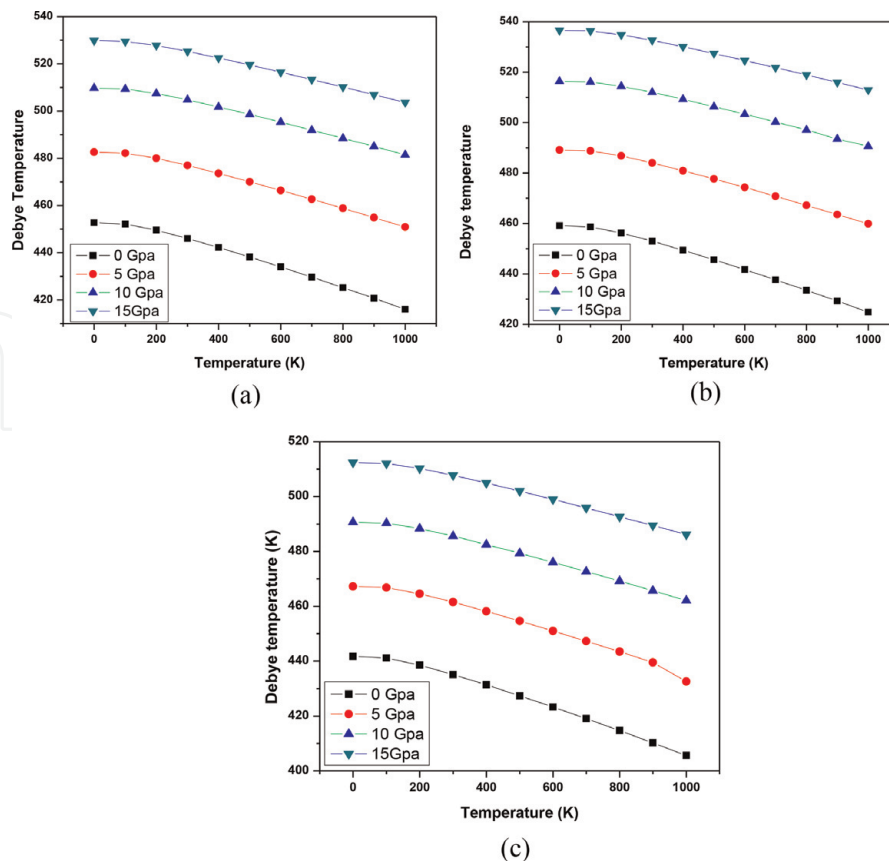


Figure 11.
 Dependence of Debye temperature (θ_D) on temperature and pressures for (a) Ba_2MgOsO_6 (b) Ba_2ZnOsO_6 (c) Ba_2CdOsO_6 .

pressure. The predicted value of (γ) at 300 K and 0 GPa of pressure is 2.088, 1.965, 2.099 respectively for Ba_2XOsO_6 ($X = Mg, Zn, Cd$).

Debye temperature (θ_D) one of the most important thermodynamic parameter helps to exposes accurate presentation of material properties like specific heat capacity and thermal expansion and also provides the decent understanding about the features of a material under the influence of temperature and pressure. The Debye temperature variation with respect to temperature/pressure is presented in **Figure 11(a–c)**. From these figures it is clear that Debye temperature shows a decreasing trend with increasing temperature and an increasing trend with increasing pressure. The calculated value of Debye temperature at 300 K and 0 GPa is 446.08, 452.97, 435.12 GPa respectively for Ba_2XOsO_6 ($X = Mg, Zn, Cd$). Some part of this work has been recently reported [53].

4. Conclusions

Ab initio calculations on electronic structure, magnetic, elastic, mechanical and thermodynamic properties of cubic double perovskite oxides Ba_2XOsO_6 ($X = Mg, Zn, Cd$) Ba_2ZnOsO_6 have been reported within density functional theory via full potential linearized augmented plane wave (FP-LAPW) method. The structural investigation reveals the ferromagnetic phase stability for these compounds. The spin polarized electronic and magnetic properties were calculated within generalized gradient approximation (GGA), Hubbard approximation (GGA + U) and mBJ (modified Becke-Johnson approximation). The electronic profile establishes half-metallic nature for these compounds and hence can strength the modern technological domain in terms of spintronic materials. The calculated total spin magnetic moment was found equal to $2 \mu_B$ for all the three compounds. Thus these materials are also looked for magnetic materials. The elastic constants have been calculated and used to predict mechanical stuffs like Shear modulus (G) Poisson ratio (ν) and anisotropic factor (A). The calculated B/G and Cauchy pressure ($C_{12}-C_{44}$) both characterize the material as brittle. The thermodynamic parameters like heat capacity and Debye temperature have also been predicted in the temperature range of 0–1000 K.


Author details

Sajad Ahmad Dar

Department of Physics, Govt. Motilal Vigyan Mahavidyalya College, Bhopal, Madhya Pradesh, India

*Address all correspondence to: sajad54453@gmail.com

IntechOpen

© 2019 The Author(s). Licensee IntechOpen. This chapter is distributed under the terms of the Creative Commons Attribution License (<http://creativecommons.org/licenses/by/3.0>), which permits unrestricted use, distribution, and reproduction in any medium, provided the original work is properly cited. 

References

- [1] Pilania G, Balachandran PV, Kim C, Lookman T. Finding new perovskite halides via machine learning. *Frontiers in Materials*. 2016;**3**:13285
- [2] Moore EA. Computational modelling of inorganic solids. *Annual Reports on the Progress of Chemistry, Section A: Inorganic Chemistry*. 2008;**104**:46
- [3] Kobayashi KI, Kimura T, Sawada H, Terakura K, Tokura Y. Room-temperature magnetoresistance in an oxide material with an ordered double-perovskite structure. *Nature*. 1998;**395**:677
- [4] Iliev MN, Padhan P, Gupta A. Temperature-dependent Raman study of multiferroic Bi_2NiMnO_6 thin films. *Physical Review B*. 2008;**77**:172303
- [5] Fiebig M, Lottermoser T, Frohlich D, Goltsev AV, Pisarev RV. Observation of coupled magnetic and electric domains. *Nature*. 2002;**419**:818
- [6] Das H, De Raychaudhury M, Saha-Dasgupta T. Moderate to large magneto-optical signals in high T_c double perovskites. *Applied Physics Letters*. 2008;**92**:201912
- [7] Krockenberger Y, Mogare K, Reehuis M, Tovar M, Jansen M, Vaitheeswaran G, et al. Sr_2CrOsO_6 : End point of a spin-polarized metal-insulator transition by 5d band filling. *Physical Review B*. 2007;**75**:020404
- [8] Feng HL, Arai M, Matsushita Y, Tsujimoto Y, Guo YF, Sathish CI, et al. High-temperature ferrimagnetism driven by lattice distortion in double perovskite Ca_2FeOsO_6 . *Journal of the American Chemical Society*. 2014;**136**: 3235
- [9] Stitzer KE, Smith MD, Loye HCZ. Crystal growth of Ba_2MOsO_6 ($M = Li, Na$) from reactive hydroxide fluxes. *Solid State Sciences*. 2002;**4**:311
- [10] Aharen T, Greedan JE, Bridges CA, Aczel AA, Rodriguez J, MacDougall G, et al. Magnetic properties of the geometrically frustrated $S = 1/2$ antiferromagnets, La_2LiMoO_6 and Ba_2YMoO_6 , with the B-site ordered double perovskite structure. evidence for a collective spin singlet ground state. *Physical Review B*. 2010;**81**:224409
- [11] de Vries MA, Mclaughlin AC, Bos J-WG. Valence bond glass on an fcc lattice in the double perovskite Ba_2YMoO_6 . *Physical Review Letters*. 2010;**104**:177202
- [12] Carlo JP, Clancy JP, Aharen T, Yamani Z, Ruff JPC, Wagman JJ, et al. Triplet and in-gap magnetic states in the ground state of the quantum frustrated fcc antiferromagnet Ba_2YMoO_6 . *Physical Review B*. 2011;**84**:100404
- [13] Wiebe CR, Greedan JE, Luke GM, Gardner JS. Spin-glass behavior in the $S=1/2$ fcc ordered perovskite Sr_2CaReO_6 . *Physical Review B*. 2002;**65**:144413
- [14] Morrow R, Freeland JW, Woodward PM. Probing the links between structure and magnetism in $Sr_{(2-x)}Ca_{(x)}FeOsO_6$ double perovskites. *Inorganic Chemistry*. 2014;**53**:7983
- [15] Paul AK, Reehuis M, Ksenofontov V, Yan B, Hoser A, Tobbens DM, et al. Lattice instability and competing spin structures in the double perovskite insulator Sr_2FeOsO_6 . *Physical Review Letters*. 2013;**111**: 167205
- [16] Kanungo S, Yan B, Jansen M, Felser C. Ab-initio study of low-temperature magnetic properties of double perovskite Sr_2FeOsO_6 . *Physical Review B*. 2014;**89**:214414

- [17] Paul AK, Jansen M, Yan BH, Felser C, Reehuis M, Abdala PM. Synthesis, crystal structure, and physical properties of $\text{Sr}_2\text{FeOsO}_6$. *Inorganic Chemistry*. 2013;**52**:6713
- [18] Ghimire MP, Hu X. Half metal transition driven by doping effects in osmium double perovskite. *arXiv preprint arXiv*. 2014;**1408**:1771
- [19] Wang H, Zhu S, Ou X, Nu H. Ferrimagnetism in the double perovskite $\text{Ca}_2\text{FeOsO}_6$: A density functional study. *Physical Review B*. 2014;**90**:054406
- [20] Dar SA, Srivastava V, Sakalle UK, Pagare G. Insight into structural, electronic, magnetic, mechanical, and thermodynamic properties of actinide perovskite BaPuO_3 . *Journal of Superconductivity and Novel Magnetism*. 2018;**31**(10):3201
- [21] Dar SA, Srivastava V, Sakalle UK, Pagare G. First-principles investigation on electronic structure, magnetic, mechanical and thermodynamic properties of SrPuO_3 perovskite oxide. *Materials Research Express*. 2018;**5**:026106
- [22] Dar SA, Srivastava V, Sakalle UK, Khandy SA, Gupta DC. A DFT study on structural, electronic mechanical and thermodynamic properties of 5f-electron system BaAmO_3 . *Journal of Superconductivity and Novel Magnetism*. 2018;**31**(01):141
- [23] Dar SA, Srivastava V, Sakalle UK. A First-principles calculation on structural, electronic, magnetic, mechanical, and thermodynamic properties of SrAmO_3 . *Journal of Superconductivity and Novel Magnetism*. 2017;**30**(11):3055
- [24] Dar SA, Srivastava V, Sakalle UK, Parey V, Pagare G. DFT investigation on electronic, magnetic, mechanical and thermodynamic properties under pressure of some EuMO_3 (M = Ga, In) perovskites. *Materials Research Express*. 2017;**4**:106104
- [25] Dar SA, Srivastava V, Sakalle UK. A combined DFT and post-DFT investigation on cubic XMoO_3 (X = Sr, Ba) perovskite oxides. *Materials Research Express*. 2017;**4**:086304
- [26] Zhao S, Wei Z, Dar SA. Insight into the Structural, Electronic, Elastic, Mechanical, and Thermodynamic Properties of XReO_3 (X = Rb, Cs, Tl) Perovskite Oxides: A DFT Study. *Zeitschrift für Naturforschung A*. 2019. DOI: 10.1515/zna-2019-0019
- [27] Dar SA, Srivastava V, Sakalle UK. High pressure and high temperature investigation of metallic perovskite SnTaO_3 . *Journal of Molecular Modeling*. 2018;**24**:52
- [28] Dar SA, Srivastava V, Sakalle UK. Ab initio high pressure and temperature investigation on cubic PbMoO_3 perovskite. *Journal of Electronic Materials*. 2017;**46**(12):6870
- [29] Cao K, Li H, Liu S, Cui J, Shen Y, Wang M. MAPbI_3 - xBr_x mixed halide perovskites for fully printable mesoscopic solar cells with enhanced efficiency and less hysteresis. *Nanoscale*. 2016;**8**:8839-8846
- [30] Chen L-C, Weng C-Y. Optoelectronic Properties of MAPbI_3 Perovskite/Titanium Dioxide Heterostructures on Porous Silicon Substrates for Cyan Sensor Applications. *Nanoscale Research Letters*. 2015;**10**:404
- [31] Colella S, Mosconi E, Fedeli P, Listorti A, Gazza F, Orlandi F, et al. MAPbI_3 - xCl_x mixed halide perovskite for hybrid solar cells: The role of chloride as dopant on the transport and structural properties. *Chemistry of Materials*. 2013;**25**:4613-4618

- [32] Ding J, Zhao Y, Du S, Sun Y, Cui H, Zhan X, et al. Polarization-dependent optoelectronic performances in hybrid halide perovskite MAPbX₃ (X = Br, Cl) single-crystal photodetectors. *Journal of Materials Science*. 2017;52:7907-7916
- [33] Najeeb MA, Ahmad Z, Shakoor RA, Alashraf A, Bhadra J, Thani NA, et al. Growth of MAPbBr₃ perovskite crystals and its interfacial properties with Al and Ag contacts for perovskite solar cells. *Optical Materials*. 2017;73:50
- [34] Lu H, Zhang H, Yuan S, Wang J, Zhan Y, Zheng L. An optical dynamic study of MAPbBr₃ single crystals passivated with MAPbCl₃/I₃-MAPbBr₃ heterojunctions. *Physical Chemistry Chemical Physics*. 2016:1-3
- [35] Chen L-C, Tseng Z-L, Huang J-K. A Study of inverted-type perovskite solar cells with various composition ratios of (FAPbI₃)_{1-x}(MAPbBr₃)_x. *Nanomaterials*. 2016;6:183
- [36] Yuan S, Wang J, Yang K, Wang P, Zhang X, Zhan Y, et al. High efficiency MAPbI_{3-x}Cl_x perovskite solar cell via interfacial passivation. *Nanoscale*. 2018; 10:18909-18914
- [37] Marjerrison CA, Thompson CM, Sharma AZ, Hallas AM, Wilson MN, Munsie TJS, et al. Magnetic ground states in the three Os₆₊ (5d₂) double perovskites Ba₂MOsO₆ (M=Mg, Zn, and Cd) from Néel order to its suppression. *Physical Review B*. 2016;94:134429
- [38] Dar SA, Srivastava V, Sakalle UK, Pagare G. Insight into electronic structure, magnetic, mechanical and thermodynamic properties of double perovskite Ba₂MgReO₆: A first-principles investigation. *Computational Condensed Matter*. 2018;14:137-143
- [39] Merabet B, Alamri H, Djermouni M, Zaoui A, Kacimi S, Boukortt A, et al. Optimal bandgap of double perovskite La-substituted Bi₂FeCrO₆ for Solar Cells: An ab initio GGA+U Study. *Chinese Physics Letters*. 2017;34(1):016101
- [40] Dar SA, Srivastava V, Sakalle UK. Structural, elastic, mechanical, electronic, magnetic, thermoelectric and thermodynamic investigation of half metallic double perovskite oxide Sr₂MnTaO₆. *Journal of Magnetism and Magnetic Materials*. 2019;484:298-306
- [41] Sahnoun O, Bouhani-Benziane H, Sahnoun M, Driz M. Magnetic and thermoelectric properties of ordered double perovskite Ba₂FeMoO₆. *Journal of Alloys and Compounds*. 2017;714:704
- [42] Dar SA, Sharma R, Srivastava V, Sakalle UK. Investigation on the electronic structure, optical, elastic, mechanical, thermodynamic and thermoelectric properties of wide band gap semiconductor double perovskite Ba₂InTaO₆. *RSC Advances*. 2019;9:9522
- [43] Dar SA, Srivastava V, Sakalle UK. Ab-initio DFT based investigation of double perovskite oxide Ba₂CdOsO₆ with cubic structure. *Computational Condensed Matter*. 2019;18:e00351
- [44] Thompson CM, Marjerrison CA, Sharma AZ, Wiebe CR, Maharaj DD, Sala G, et al. Frustrated magnetism in the double perovskite La₂LiOsO₆: A comparison with La₂LiRuO₆. *Physical Review B*. 2016;93:014431
- [45] Dar SA, Srivastava V, Sakalle UK, Parey V, Pagare G. A combined DFT, DFT+U and mBJ investigation on electronic structure, magnetic, mechanical and thermodynamics of double perovskite Ba₂ZnOsO₆. *Materials Science and Engineering B*. 2018; 236-237:217-224
- [46] Faizan M, Khan SH, Murtaza G, Khan A, Khenata R, Mahmood A, et al. Structural, elastic, electronic and magnetic properties of Ba₂XOsO₆ (X = Li, Na, Ca) double perovskites. *Indian Journal of Physics*. 2016;90:1225

- [47] Dar SA, Srivastava V, Sakalle UK, Parey V. Electronic structure, magnetic, mechanical and thermo-physical behavior of double perovskite $\text{Ba}_2\text{MgOsO}_6$. *European Physical Journal Plus*. 2018;**133**:64
- [48] Otero-de-la-Roza A, Abbasi-Perez D, Luaea V. Gibbs2: A new version of the quasiharmonic model code. II. Models for solid-state thermodynamics, features and implementation. *Computer Physics Communications*. 2011;**182**:2232
- [49] Otero-de-la-Roza A, Luaea V. Equations of state and thermodynamics of solids using empirical corrections in the quasiharmonic approximation. *Physical Review B*. 2011;**84**:184103
- [50] Wu Z, Cohen RE. More accurate generalized gradient approximation for solids. *Physical Review B*. 2006;**73**:235116
- [51] Blaha P, Schwarz K, Madsen GKH, Kuasnicke D, Luitz J. Introduction to WIEN2K, an Augmented Plane Wave plus Local Orbitals Program for Calculating Crystal Properties. Vienna, Austria: Vienna University of Technology; 2001
- [52] Perdew JP, Burke K, Ernzerhof M. Generalized gradient approximation made simple. *Physical Review Letters*. 1996;**77**:3865
- [53] Tran F, Blaha P. Accurate band gaps of semiconductors and insulators with a semilocal exchange-correlation potential. *Physical Review Letters*. 2009;**102**:226401
- [54] Petukhov AG, Mazin II. Correlated metals and the LDA+U method. *Physical Review B*. 2003;**67**:153106
- [55] Novak P, Kunes J, Chaput L, Pickett WE. Exact exchange for correlated electrons. *Physica Status Solidi B: Basic Solid State Physics*. 2006;**243**:563
- [56] Aisimov VI, Solovye IV, Korotin MA, Czyzyk MT, Sawatzky GA. Density-functional theory and NiO photoemission spectra. *Physical Review B*. 1993;**48**:16929
- [57] Hou YS, Xiang HJ, Gong XG. Lattice-distortion induced magnetic transition from low-temperature antiferromagnetism to high-temperature ferrimagnetism in double perovskites A_2FeOsO_6 ($\text{A} = \text{Ca}, \text{Sr}$). *Scientific Reports*. 2015;**5**:13159
- [58] Monkhorst HJ, Pack JD. Special points for Brillouin-zone integrations. *Physical Review B*. 1976;**13**:5188
- [59] Charpin T. A Package for Calculating Elastic Tensors of Cubic Phases Using WIEN. Paris, France: Laboratory of Geometrix F-75252; 2001
- [60] Birch F. The effect of pressure upon the elastic parameters of isotropic solids, according to Murnaghan's theory of finite strain. *Journal of Applied Physics*. 1938;**9**:279
- [61] Dimitrovska S, Aleksovska S, Kuzmanovski I. Prediction of the unit cell edge length of cubic $\text{A}_2^{2+}\text{BB}'\text{O}_6$ perovskites by multiple linear regression and artificial neural networks. *Central European Journal of Chemistry*. 2005; **3**(1):198
- [62] Mehl MJ, Klein BK, Papaconstantopoulos DA. (Intermetallic compounds); principle and practice. In: Westbrook JH, Fleischeir RL, editors. *Principles*. Vol. 1. John Wiley and Sons; 1995
- [63] Voigt W. *Lehrbush der Kristallphysik*. Leipzig: Taubner; 1928
- [64] Schreiber E, Anderson OL, Soga N. *Elastic Constants and Measurements*. New York: M.C Graw Hill; 1973
- [65] Hill R. The elastic behaviour of a crystalline aggregate. *Proceedings of the Physical Society (London)*. 1952;**65**:349

[66] Pugh SF. Relations between the elastic moduli and the plastic properties of polycrystalline pure metals. *Philosophical Magazine*. 1954;**45**:823

[67] Petit AT, Dulong PL. Sur quelques points importants de la théorie de la chaleur. *Annales de Chimie Physique*. 1819;**10**:395

[68] Quiang L, Duo-Hui H, Qi-Long C, Fan-Hou W. Phase transition and thermodynamic properties of BiFeO₃ from first-principles calculations. *Chinese Physics B*. 2013;**22**:037101

IntechOpen